Waste-tyre pyrolysis and gasification via the reverse Boudouard reaction: derivation of empirical kinetics from TGA data

Arnold Alexander Jansen[a,b], Izak Jacobus van der Walt[b], Philippus Lodewyk Crouse[a]

[a]Department of Chemical Engineering, University of Pretoria, Pretoria 0002, South Africa, [b]South African Nuclear Energy Corporation SOC Limited, Elias Motsoaledi Street Extension R104, Pelindaba, Brits 0240, South Africa.

aaj421216@gmail.com Postal address: P.O Box 257, Ifafi 0260, Rep. of South Africa.

Abstract: The pyrolysis of scrap tyre rubber crumbs under nitrogen and treatment with pure carbon dioxide was investigated both iso-thermally and dynamically up to 1100 °C, at heating rates up to 20 °C min^{-1}. The rubber sample was a mixture of industrially representative tread and sidewall material. Workable, but not definitive, models could be derived from the iso-thermal analysis: 3D diffusion for the first pyrolysis event under nitrogen up to 550 °C; the Mampel mechanism for high-temperature pyrolysis above 550 °C; and shrinking-particle chemical-reaction control as the rate limiting step for the reverse Boudouard reaction. The iso-thermally derived pre-exponential factors and activation energies were further refined by non-linear fitting to the dynamic data of all heating rates, and by making both parameters functions of the degree of conversion. In addition, the Sestak-Berggren equation was directly fitted to the full data set, i.e., for all heating rates, also using pre-exponential factors and activation energies that are dependent on degree of conversion. Both the approaches yielded workable engineering kinetics, with the Sestak-Berggren performing worse. With single-value pre-exponential factors and activation energies, the models fitted the data less satisfactorily across the range of heating rates. The required numerical analysis is fully implementable on a commercial spreadsheet.

Keywords: reverse Boudouard reaction; pyrolysis; gasification; kinetics; waste tyres; TGA.

1 Introduction

Globally about 1.6 billion new tyres are manufactured each year and about 1 billion are scrapped; of these only an estimated 100 million are processed by the recycling industry [1]. Consequently, the disposal, recycling, re-purposing, and the recovery of useful products and energy from end-of-life tyres (ELT) have received wide-spread attention over many years. Tyres are non-biodegradable and stockpiling creates health-, pollution- and fire hazards [2,3]. Worn tyres are recycled mainly for granulation or for energy recovery, predominantly in cement kilns and the paper and pulp industry. They are also recovered for civil engineering applications or retreaded and a percentage was previously land-filled, now no longer an option. Most tyres, however, are stockpiled [4-7].

There are three main thermal treatment processes for waste tyres: combustion as tyre-derived fuel (TDF); pyrolysis for the recovery of valuable products like char, oils, and light hydrocarbons; and gasification for the production of synthesis gas for power generation or chemical synthesis. Under controlled combustion conditions its high heating value (> 30 MJ/kg) makes TDF attractive for energy production in cement kilns, the paper and pulp industry, and boilers [8,9]. In fact, TDF in cement kilns produces 25 % more energy than the equivalent amount of coal [10] and can lower NO_x emissions [11]. Pyrolysis and gasification of ELT have been widely researched as alternatives to their use as TDF. Several reviews have been published in this regard [8,12-27].

Gasification can also be carried out with CO_2 using the reverse Boudouard reaction at temperatures above 700 °C and various mechanisms and models have been proposed and reviewed [28-38]. This provides a method of recycling CO_2 to yield usable CO, either for syngas or energy provision, and thus is a step towards carbon neutrality. Of particular interest for this work, plasma-assisted gasification with CO_2 has been investigated [39-42] and a high-efficiency, high enthalpy plasma torch operating on CO_2 has been developed [43,44]. Steam plasmas are characterized by very high gas enthalpy and generated by means of, e.g., Gerdien-type water-stabilized arc discharges [43-47] and microwave plasmas [48,49] have also been used for the gasification of ELT.

The South African Nuclear Energy Corporation Ltd. (Necsa) has had an interest in plasma technology since the 1980s, with an initial emphasis on nuclear-related processes. More recently they have invested research funding into plasma-based treatment and gasification of non-nuclear waste [50-54]. To date, demonstrators for municipal solid waste and biomass have been developed, ranging in size from 100 to 500 kg feed per day. They are currently in a design optimization phase for piloting larger systems. The research reported here forms part of this gasification development program, targeting waste tyres as feed material to produce CO-rich synthesis gas, suitable for use in electrical generator equipment, using carbon dioxide as the main oxidizing medium. The gasification is done in semi-batch mode, using a non-transfer plasma torch as heat source to maintain the ceramic-lined reactor at a temperature in the range 1000–1100 °C, with the rubber crumbs fed into the torch tailflame. One of the main objectives to assist with the design of the plasma-assisted gasification reactor, is to generate chemical kinetic data to incorporate into heat transfer models for single macroscopic tyre particles. The kinetic parameters need to be of reasonable engineering quality and address a range of heating rates.

During gasification, the rubber undergoes initial pyrolysis, devolatilization, and gas-phase reactions, followed by char formation and then gas-solid reactions consuming the char. Several reports are available in the open literature addressing these conditions and using different oxidising species. They are discussed in more detail in Section 3 below. However, apart from the need for having measured data for the target material used in

this study, we require the kinetic parameters to describe non-overlapping events for ease of programming into heat-transfer models. For example, the low-temperature pyrolysis step, whether under N_2 or CO_2, is characterized by several overlapping events, specific to the exact composition of the rubber. We wanted to generate a single set of parameters, i.e., a single triplet, for the full pyrolysis event, and another for the full reverse Boudouard reaction, and to test these triplets against the experimental data for the various heating rates studied.

For the work reported here, the thermal behaviour of waste rubber of local industrial interest was investigated using both dynamic and isothermal thermogravimetric analysis (TGA). Data processing was solely spreadsheet based. The novelty of the work lies in the testing of the isothermal kinetics on dynamic data, and the method presented for direct fitting of models across all heating rates and should be of interest to researchers in rubber pyrolysis and gasification.

2 Materials and methods

2.1 Materials

The tyre sample used in this study was procured from Mathé Group (Pty) Ltd, a commercial supplier in South Africa. They granulate all brands of truck tyres, without segregation, into a 1.0 to 5.0 mm size with in-situ removal of the metal and residual polymer. The complete tyre is shredded without separating the tread from the side wall. The specific sample number identifier was: Premium Granulated Rubber (MRC 1,0–5,0.025.200). The average bulk density of this material was 0.45 kg/m^3. To obtain reasonable rubber sample homogeneity, all material used was frozen in liquid-nitrogen and ground in an electric blade-grinder. This material was sieved to accumulate the <100 μm fraction. The proximate analysis for the materials indicated: moisture < 1 %; volatiles 66–68 %; carbonaceous material 23–25 %; ash 7–8 %. The ultimate analysis indicated the following values: C 82.97 %; H 7.06 %; N 0.04 %; S 1.33 %, with ash making up the difference. Nitrogen (4N) and carbon dioxide (3N), obtained from Afrox Pty Ltd, were used in the TGA experiments.

2.2 Instrumentation and sample preparation

All thermal analysis experiments were executed using a Hitachi STA7300 horizontal-beam TGA-DTA system. Alumina crucibles, 5 mm H × 6 mm OD, were used in all cases. Gas flow was kept constant at 20 cm^3 min^{-1}. Although the signal-to-noise ratio of the instrument is sufficiently high to obtain good results down to 1 mg for a single sample, only sample sizes above ~20 mg gave consistent results, due to the inherent inhomogeneity of the original sample. This was a necessary trade off against non-uniform results.

2.3 Data processing

Thermal analysis is a well-established technique, and the mathematical interpretation of thermograms dates from well before the current era of high-performance desktop computers. Indeed, the first review on TGA curve fitting was published in 1960 [55]. For this work the guidelines provided by the Kinetics Committee of the International Confederation for Thermal Analysis and Calorimetry (ICTAC) [56,57] were broadly followed.

The extraction of kinetic data from reaction data is, per definition, the determination of the kinetic triplet, i.e., the model $f(\alpha)$, the activation energy E_A, and the pre-exponential factor k_0, as contained in the differential rate law:

$$\frac{\mathrm{d}\alpha}{\mathrm{d}t} = f(\alpha)k(T) = f(\alpha)k_0 e^{-\frac{E_A}{RT}} \quad (1)$$

T and t are absolute temperature and time respectively, and R the ideal gas constant. The degree of conversion, α, is expressed as

$$\alpha = \frac{m_0 - m(t)}{m_0 - m_{Fin}} \quad (2)$$

Here m_0 is the starting mass of the sample, $m(t)$ is the sample mass at time t, and m_{Fin} the final mass for the thermal event in question. For the reverse Boudouard reaction, m_{Fin} is the ash content. For pyrolysis, m_{Fin} for the first (low temperature) pyrolysis event was taken from the average value for a selection of representative runs. For the second pyrolysis event, m_{Fin} was the average for three runs done up to 1100 °C and maintained at that temperature for 15 min. Values of α between 0.05 and 0.95 only, were used.

The integrated form of Equation 1 is:

$$g(\alpha) = \int_0^\alpha \frac{1}{f(\alpha)} = k(T)t = \frac{t}{\tau} \quad (3)$$

Here τ is the time for the reaction to reach completion.

Isothermal runs for the first and second pyrolysis events were performed under pure nitrogen, and under CO_2 for the high temperature (>550 °C) reverse Boudouard reaction. The temperatures for these runs were selected based on observations from dynamic runs. For pyrolysis, the selection of a solid-state model was restricted to the 14 listed in **Error! Reference source not found.**. The models for the reverse Boudouard reaction were restricted to the three gas-solid models listed in **Error! Reference source not found.**.

Table 1: Kinetics models used for solid-state reactions [57].

	Reaction model	**Code**	$f(\alpha)$	$g(\alpha)$
1	Power law	P4	$4\alpha^{3/4}$	$\alpha^{1/4}$
2	Power law	P3	$3\alpha^{2/3}$	$\alpha^{1/3}$
3	Power law	P2	$2\alpha^{1/2}$	$\alpha^{1/2}$
4	Power law	P2/3	$2/3\alpha^{-1/2}$	$\alpha^{3/2}$
5	Mampel (first order)	F1	$1-\alpha$	$-\ln(1-\alpha)$
6	Avrami-Erofeev	A4	$4(1-\alpha)[-\ln(1-\alpha)]^{3/4}$	$[-\ln(1-\alpha)]^{1/4}$
7	Avrami-Erofeev	A3	$3(1-\alpha)[-\ln(1-\alpha)]^{2/3}$	$[-\ln(1-\alpha)]^{1/3}$
8	Avrami-Erofeev	A2	$2(1-\alpha)[-\ln(1-\alpha)]^{1/2}$	$[-\ln(1-\alpha)]^{1/2}$
9	Contracting sphere	R3	$3(1-\alpha)^{2/3}$	$1-(1-\alpha)^{1/3}$
10	Contraction cylinder	R2	$2(1-\alpha)^{1/2}$	$1-(1-\alpha)^{1/2}$
11	One-dimensional diffusion	D1	$1/2\alpha^{-1}$	α^2
12	Two-dimensional diffusion	D2	$[-\ln(1-\alpha)]^{-1}$	$(1-\alpha)\ln(1-\alpha)$
13	Three-dimensional diffusion (Jander)	D3	3	$[1-(1-\alpha)^{1/3}]^2$
14	Three-dimensional diffusion (Ginstling-Brounshtein)	D4	$3/2[(1-\alpha)^{-1/3}-1]^{-1}$	$1-2/3\,\alpha$

Table 2: Kinetics models used for gas-solid reactions [58].

	Reaction model	**Code**	$\mathbf{d\alpha/dt} = f(\alpha)/\tau$	$g(\alpha) = t/\tau$	τ
1	Gas-film diffusion control	L1	1	α	$\frac{\rho_B R}{3bk_g C_{Ag}}$
2	Ash-layer diffusion control	L2	$[2(1-\alpha)^{-1/3}-(1-\alpha)^{-1}]^{-1}$	$1-3(1-\alpha)^{2/3}+2(1-\alpha)$	$\frac{\rho_B R}{6bD_e C_{Ag}}$
3	Contracting sphere with chemical reaction control	L3	$3(1-\alpha)^{2/3}$	$1-(1-\alpha)^{1/3}$	$\frac{\rho_B R}{bk" C_{Ag}}$

Notes: Levenspiel's symbols are used. R is the radius of the solid particle, ρ_B is its density, C_{AG} is the concentration of the reacting gas, and b is the stoichiometric coefficient for reaction normalized with respect to the solids, i.e., Fluid + bSolid → Products, k_g and $k"$ are rate constants, and D_e is the diffusion coefficient of the gas through the ash layer.

For iso-thermal analysis, the integral form of the models was plotted as function of time, with the test for optimal linearity, i.e., the highest value for R^2, determining the most suitable model. For these plots the starting time was taken at the point when the temperature appeared to have reached steady state. Subsequent to the initial fit, the time points were zero-shifted by the addition of the intercept/slope quotient. The

temperature-dependent values of the rate constants were determined from the slopes. The all-temperature R^2 values obtained for each the linear model fits for any given model, were used as input for an analysis of variance (ANOVA, [59]) to select the most appropriate model. The activation energy and pre-exponential terms for the model of choice were then obtained from Arrhenius plots. These values were subsequently refined by using them as initial values for direct non-linear fitting to the full dynamic TGA data set, employing the model determined for each event.

In addition, a direct non-linear model fitting method was followed for analysis of the dynamic data, using the combined data sets for all heating rates for each thermal event. The Sestak-Berggren (S-B) equation (4) was used:

$$f(\alpha) = \alpha^m(1-\alpha)^n[-\ln(1-\alpha]^p \quad (4)$$

Despite the generality and flexibility of the S-B, it was found to be unable to provide an adequate fit across the full set of heating rates. The final fit would invariably favour either the low-, the middle-, or high heating-rate thermograms. The models obtained from the isothermal analysis, similarly, did not provide a satisfactory fit to the full heating-rate range. After an initial less than satisfactory attempt to introduce a temperature dependence for the pre-exponential factor and the activation energy, the best results were obtained by making them functions of the degree of conversion. The expression for the rate constant was modified to

$$k(T,\alpha) = k_0 e^{q\alpha} e^{-\frac{E_A(1-r\alpha)}{RT}} \quad (5)$$

with both r restricted to the range 0–1, and $q \geq 0$. In many cases the two values reached very small final values, making the approximation a numerical optimization aid, rather than providing a wide range for the two kinetic parameters. The data were processed in Microsoft Excel, and parameter optimization was done using the Solver add-in [60]. The overall algorithm, embedded in the spreadsheet, is illustrated in Figure 1 below. For the analysis process the heating rate $\beta = \mathrm{d}T/\mathrm{d}t$ is substituted into Equation 1, to yield:

$$\frac{\mathrm{d}\alpha}{\mathrm{dT}} = \frac{1}{\beta}\mathrm{f}(\alpha)k(T,\alpha) = \frac{1}{\beta}f(\alpha)k_0 e^{q\alpha} e^{-\frac{E_A(1-r\alpha)}{RT}} \quad (6)$$

Eulers's method, the simplest of numerical integration algorithms, was found to be adequate for integrating Equation 6:

$$\alpha_{i+1} = \alpha_i + \frac{1}{\beta}f(\alpha_i)k_0 e^{q\alpha_i} e^{-\frac{E_A(1-r\alpha_i)}{RT_i}} \delta T \quad (7)$$

The calculational sequence is: read the estimated values for the kinetic parameters, with the assumption that the identical set applies to all heating rates; read the minimum values for the objective function (OF) to define convergence; integrate the model equation for each heating rate; for each data set compute the absolute

average error (AAE) between experimental data points and model data points and calculate the OF as the unweighted sum of these AAEs. If the OF does has not reached the minimum value set, the parameters are adjusted, and the process is repeated. The process stops when the minimum value specified for the OF is reached.

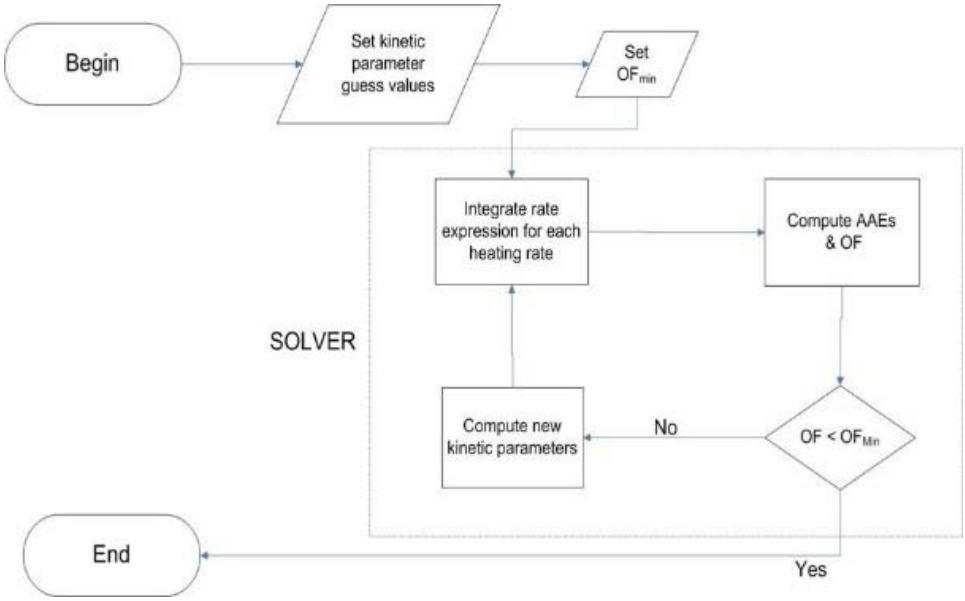

Figure 1: Non-linear curve fitting flowsheet.

Starting parameter values across all heating rates were obtained by fitting models for each of the heating rates individually and average values then calculated for each parameter, to be used as initial guesses.

The length of the text file representing the thermograms varied between 3 000 and 30 000 rows. Solution time, using a standard PC with an i7 chip and 8 GB RAM, took 5–20 min for each guessed value set, depending on the number of iterations specified. In general the GRG Non-linear scheme of the Microsoft Excel Solver add-in was adequate. Ad hoc constraints for the parameters were used when the optimization process went in an obviously wrong direction, e.g., when they became negative.

2.4 Experimental planning

Dynamic TGA analyses were performed at heating rates between 2 and 20 °C min^{-1}, in both nitrogen and pure carbon dioxide atmospheres. Isothermal analyses were conducted subsequently for three temperature ranges, viz., 200–350 °C and 600–1000 °C under nitrogen, and 720–920 °C under carbon dioxide. These ranges were determined by trial and error. Excessively high temperatures gave values of α which were too high at the start of the run, with too short a reaction period at the isothermal temperature. Dynamic pyrolysis under carbon dioxide appeared identical to the nitrogen case and was not addressed separately as an iso-

thermal case. Fitting of the dynamic data only was done. For the iso-thermal analyses the temperature was ramped up to the desired temperature at 80 °C min^{-1}. In practice the stable control region was 3–5 °C wide.

3 Results and discussion

A large body of work on the pyrolysis of ELT is available in the open literature, as evidenced by the reviews referred to in Section 1. The formation and composition of the products are influenced by the temperature, particle size, feed rate, heating rate, gas residence time and reactor type [61,62]. The thermal degradation of the rubber components is due to depolymerization [63] and cracking of the volatile products. The product composition of the different fractions can differ markedly, depending on the origin of the ELT, the temperature [64], and whether the sample originates from the tread or sidewall [65]. In the present study commercial samples, mixtures of tread and sidewall rubber, were used.

Pyrolysis begins at around 250 °C with the formation of tars and tyre pyrolysis oil (TPO) consisting of a complex mixture of C_5–C_{10}, and higher, hydrocarbons [66-70]. As the temperature rises above about 475 °C the hydrocarbons are progressively converted to aromatic compounds via Diels-Alder type reactions and eventually at around 600 °C, to the gaseous phase consisting of mainly C_1–C_4 hydrocarbons, CO_2, and minor amounts of CO, H_2S and H_2, reaching a maximum yield at 800 °C [62,71-73]. Sulphur is present in ELT as thiophenes and inorganic sulphides. During pyrolysis S is found in tars, followed by significant H_2S formation between 500 °C and 700 °C. Above 800 °C almost 50 % of the sulphur can be found in the char in the form of sulphides and sulphates [64,74,75].

It has been claimed that pyrolysis under CO_2 significantly suppresses the formation of polyaromatic hydrocarbons (PAH), indicating two different pathways in CO_2 and N_2 atmospheres [76]. The disproportionation reaction of CO to form carbon and CO_2 was first described by Octave Boudouard when he applied Le Chatelier's principle to carbon and its oxides [77]:

$$2CO(g) \rightleftharpoons CO_2(g) + C(s) \quad (8)$$

The reverse reaction may be used in the gasification of carbonaceous materials at temperatures above 700 °C. The thermodynamically predicted equilibrium composition for the stoichiometric reaction is illustrated in Figure 2 below. The reaction is endothermic and driven by the accompanying change in entropy. In practice the reaction only becomes noticeable above ~700 °C.

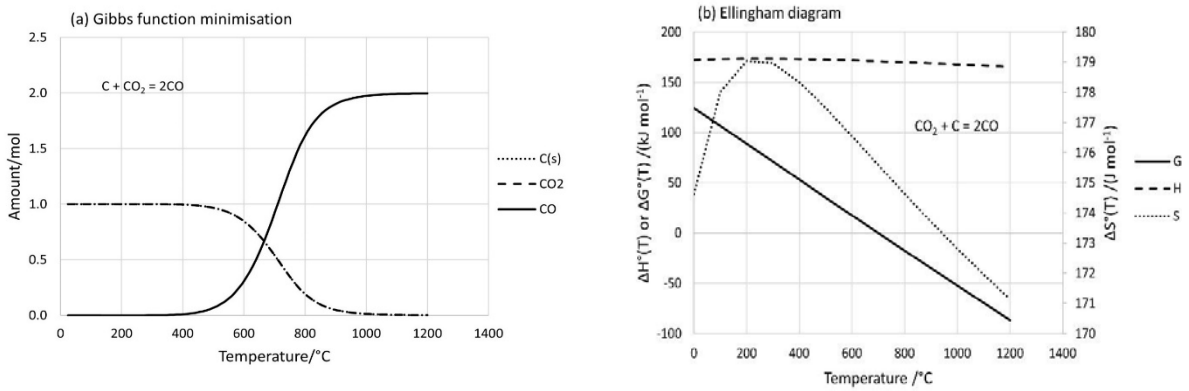

Figure 2: Reverse Boudouard reaction: equilibrium speciation curve for the stoichiometric reaction between graphite and carbon dioxide and the entropy and enthalpy contributions to the change in Gibbs energy for the reaction.

Kinetic models for the reverse Boudouard reaction are available and generally take the quality of the solid into account. Strictly speaking the phrase Boudouard reaction refers to the reversible disproportionation of CO_2 to form CO and pure carbon, not tar. We use the expression thus somewhat loosely to include tar. The char surface characteristics have been considered [31], as well as the compensating effect of catalytic elements [33], and the disintegration of the char particles to account for a rise in reaction rate, after a critical level of conversion has been achieved [38]. Scott and co-authors [36] reported difficulties with the friability of tyre chars which would support this view. The work of Struis and co-authors [37] on the catalytic effects of metals on the gasification rate of charcoal suggests that the presence of Zn in the matrix inhibits its reactivity towards CO_2 over the entire conversion range in the reaction-controlled regime (800 °C). One might suspect that the same applies to the case of tyre-derived chars where Zn is present in the ash. According to Calo and Perkins [28] the heterogeneous surface model (HSM) in the chemically controlled region, coupled to an oxygen exchange process, agrees well with the steady state kinetics of the Boudouard reaction. However, it may not hold for all chars under all conditions, and they are of the opinion that it may be impossible to obtain a true rate constant for the reaction. The oxygen exchange mechanism originally suggested by Ergun [29] is still widely used [36]. The work by Issac and co-authors [30] showed that gasification of tyre char with CO_2 exhibits a reaction order of 0.62 at 1000 °C, increasing to 0.92 at 1300 °C, indicating a transition to diffusion control. The material was macroporous and had low reactivity. The catalytic effect of ash components was only evident at temperatures below 1000 °C.

The raw data with respect to the dynamic pyrolysis under N_2 and the reaction with CO_2, are found in Figure 3 below. These results indicate that up to about 800 °C the thermal degradation of ELT under N_2 and CO_2 flow follows the same trend. A slow initial mass loss attributable to dehydration is followed by volatilization and incipient depolymerization up to about 300 °C after which the decomposition rate increases sharply up to 450–500 °C. The slow mass loss occurring between 500 °C and 800 °C may be attributed to the cracking and

volatilization of high-molecular-weight residuals in the char matrix. Above 800 °C under CO_2 flow the reverse Boudouard reaction volatilizes the char, with the rate increasing as the temperature rises. The general shape of the experimental TGA curves in Figure 3 and the shift to higher temperature with increasing heating rate are similar to those found in the literature, e.g., by Unapumnuk et al. [78], Seidelt et al. [79], and Cherbanski et al. [80].

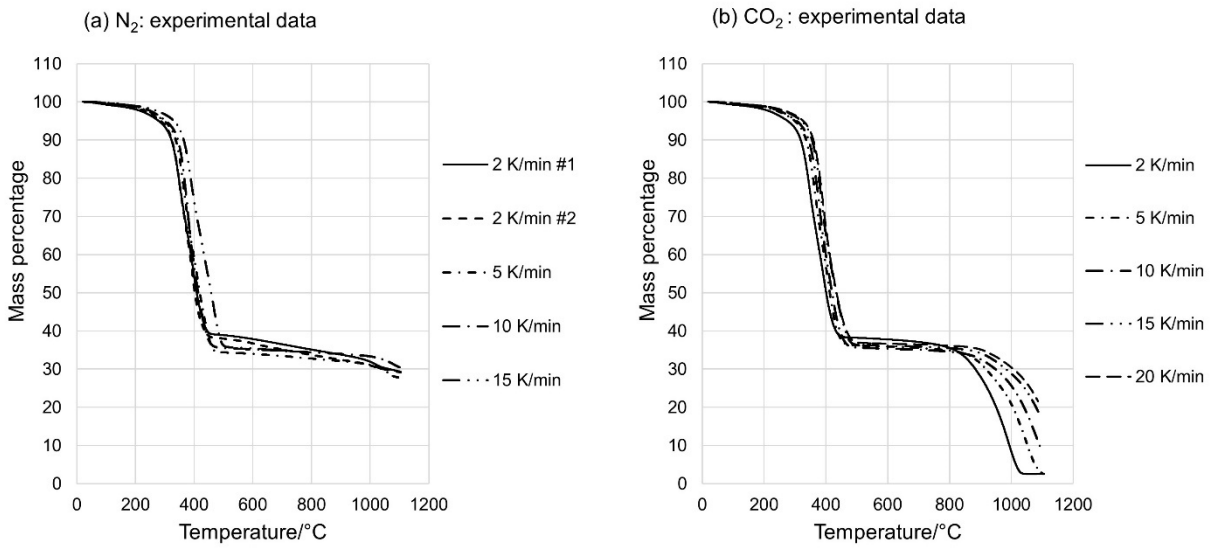

Figure 3: TGA raw data under N_2 and CO_2 flow.

The results of the isothermal kinetic analyses are given graphically in Figure 4, Figure 5 and Figure 6 below. For isothermal pyrolysis an R^2 value was calculated for each of the temperatures at which data were collected, for each of the 14 solid-state models in Table 1. The linearized integrated forms of the rate laws were used here. The uncertainty for each of the runs was assumed to fold into the average R^2 for each model. The results of an ANOVA analysis at the temperatures for which data were collected for each model, are given in Table 3, below. Only for the low-temperature pyrolysis event under nitrogen (Figure 4), the F value > F_{crit}, and $P < 0.05$; thus, only for this case there is a statistically significant difference in variance amongst models. The diffusion model D3 has the highest R^2 value and therefore selected as the model of choice, although a pair-wise set of t-tests revealed no statistical difference amongst the four diffusion models. The selection of D3 is therefore not statistically strong and the model is chosen using the highest average R^2 as metric. The conclusion here is that mass transfer is the rate determining mechanism, without the ability to pinpoint the exact nature of the diffusion in question.

For high-temperature pyrolysis under both N_2 (Figure 5) and for the reverse Boudouard, under CO_2 (Figure 6) there is no significant difference in variance amongst models. For these two analyses the Mampel 1st order

model, F1, and the reaction-controlled shrinking-particle model, L3, respectively were chosen on the basis of their highest calculated average R^2 values.

In the case of the reverse Boudouard reaction (Figure 6), the very large variance of L1 results in the poor statistical comparison. L3 is chosen on the basis of its highest R^2 value, as stated, and defended as the physically most viable model. Since the ash content of the rubber is very low (7–8 %) it is unlikely that the ash-layer diffusion limiting case, L2, is applicable.

Table 3: ANOVA for model selection from iso-thermal data.

	Pyrolysis <550 °C			Pyrolysis >550 °C			Reverse Boudouard			
Model	No of runs	Ave R^2	Var	Count	Ave R^2	Var	Model	No runs	Ave R^2	Var
P4	4	0.8956	0.0051	6	0.9741	0.0004	L1	6	0.9123	0.0317
P3	4	0.9015	0.0047	6	0.9763	0.0004	L2	6	0.9894	0.0004
P2	4	0.9126	0.0041	6	0.9801	0.0004	L3	6	0.9949	0.0001
P2/3	4	0.9624	0.0013	6	0.9899	0.0002				
F1	4	0.9593	0.0008	6	0.9931	0.0001				
A4	4	0.9124	0.0024	6	0.9845	0.0002				
A3	4	0.9188	0.0021	6	0.9864	0.0002				
A2	4	0.9306	0.0017	6	0.9895	0.0001				
R3	4	0.9539	0.0011	6	0.9926	0.0001				
R2	4	0.9509	0.0013	6	0.9919	0.0001				
D1	4	0.9767	0.0006	6	0.9875	0.0001				
D2	4	0.9817	0.0003	6	0.9868	0.0001				
D3	4	0.9860	0.0001	6	0.9835	0.0001				
D4	4	0.9833	0.0002	6	0.9860	0.0001				
F			2.2450			1.1262				1.1900
F crit.			1.9612			0.3527				3.6823
P			0.0241			1.8627				0.3314

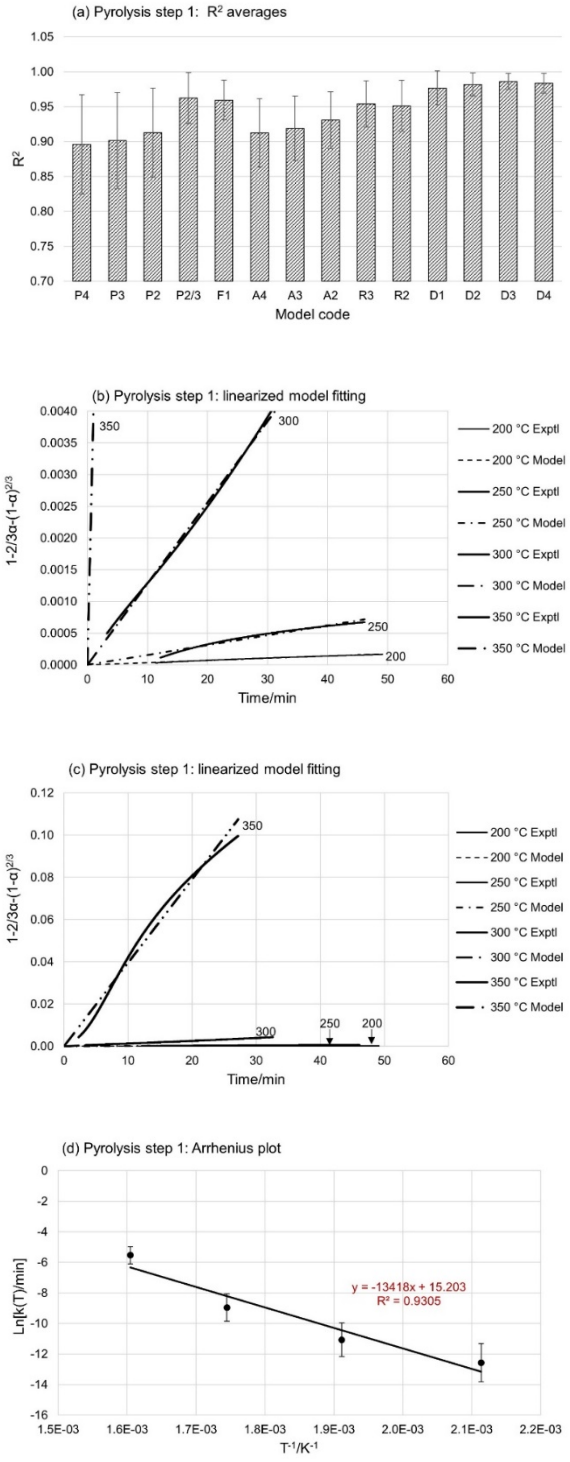

Figure 4: Derivation of the isothermal kinetics for the first pyrolysis step under N_2: (a) R^2 averages and errors across the temperature -range for each model; (b) and (c) experimental and model fitting; and (d) Arrhenius plot for model D3.

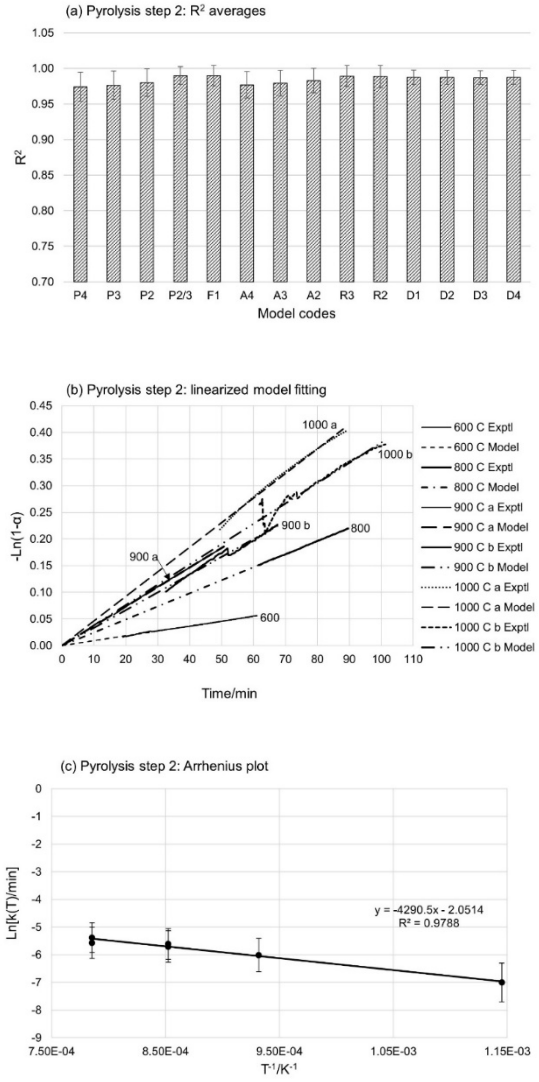

Figure 5: Derivation of the isothermal kinetics for the second pyrolysis event under N_2: (a) R^2 averages and errors across the temperature range for each model; (b) experimental and model fitting; (c) Arrhenius plot for model F1.

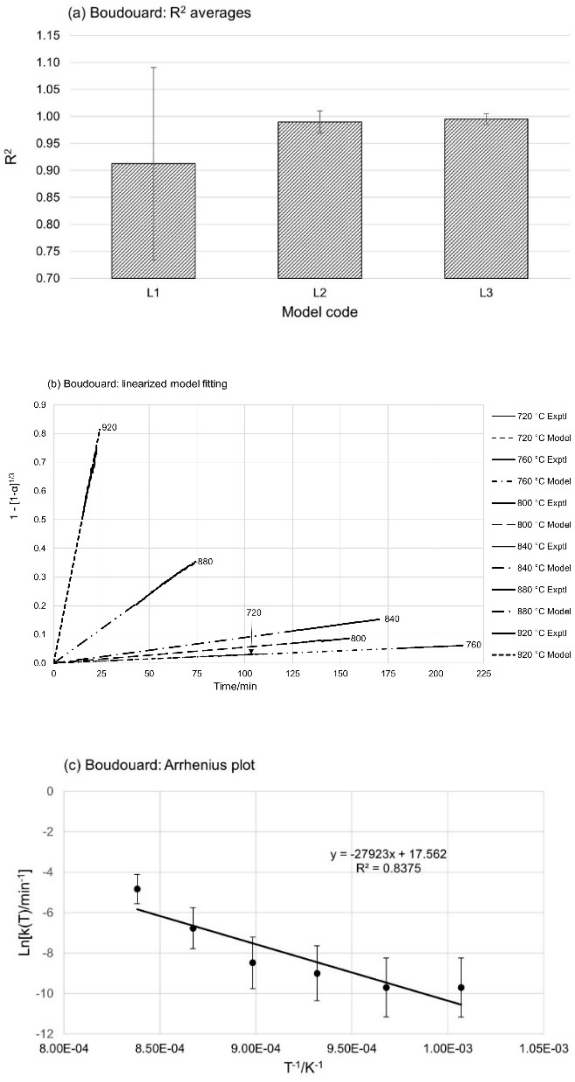

Figure 6: Derivation of the isothermal kinetics for the reverse Boudouard reaction: (a) R^2 averages and errors across the temperature range for each model; (b) experimental and model fitting; (c) Arrhenius plot for model L3.

The iso-thermal kinetic parameters derived from the Arrhenius plots in figures 4 to 6, as summarized and listed in Table 4, below, were used as the initial values for further model refinement.

Table 4: Derived iso-thermal kinetic parameters.

	Pyrolysis step 1		Pyrolysis step 2		Reverse Boudouard	
Model	D3		F1		L3	
Temperature	200–550 °C		550–1000 °C		750–1100 °C	
	Initial	Refined	Initial	Refined	Initial	Refined
q	1	0	1	5.0×10^{-2}	1	5.664×10^{-3}
k_0 (min^{-1})	4.006×10^{6}	7.337×10^{8}	1.286×10^{-1}	6.647×10^{-2}	4.232×10^{7}	2.580×10^{6}
R	1	2.578×10^{-2}	1	1.0×10^{-2}	1	0
E_A (kJ mol^{-1})	111.6	140.0	35.7	35.7	232.21	168.9

Analyses of the dynamic TG data are given in Figure 7 to Figure 11. To visually assess the goodness of fit, the development of the degree of conversion is plotted separately for each individual heating rate. The first and second pyrolysis events under nitrogen flow are given in Figure 7 and Figure 8 respectively. The thermal behaviour of the rubber under pure carbon dioxide is depicted in Figure 9 and Figure 10. Results of the model predictions obtained from non-linear optimization using the S-B, and the iso-thermally derived kinetic models, are displayed. The kinetic parameters for the derived rate expressions are listed in Table 5. To quantify goodness of fit, average absolute errors (AAEs) between model and experimental values were calculated in the range $0.05 \leq \alpha \leq 0.95$. These errors are given in Table 6. The errors are averaged over all temperatures for each reaction. Simulations of the overall mass-loss curves, combining the two events and using the iso-thermal and dynamic kinetic parameters, are given in Figure 11.

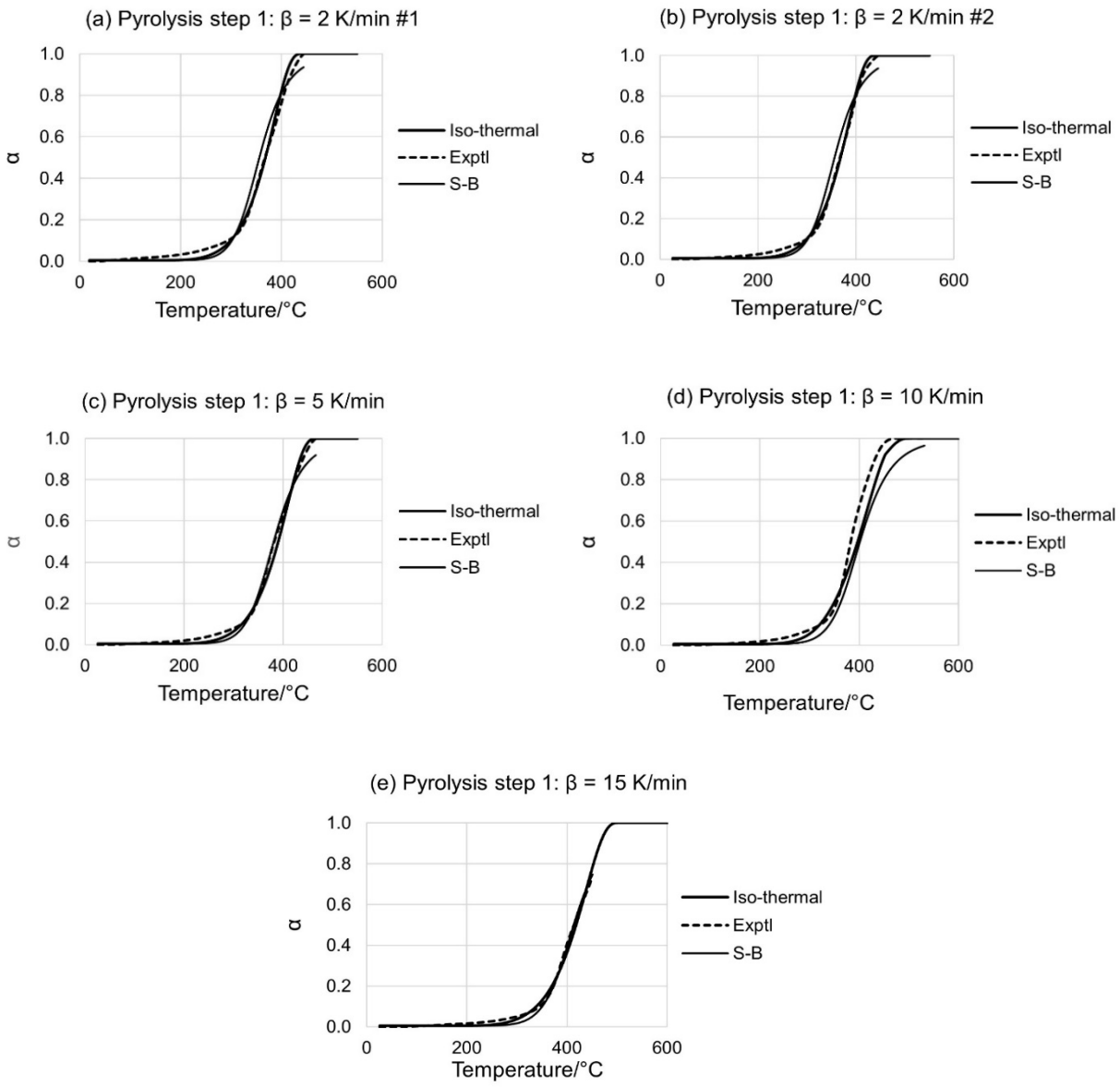

Figure 7: First thermal event under pure N_2. Curves fitted individually for each heating rate.

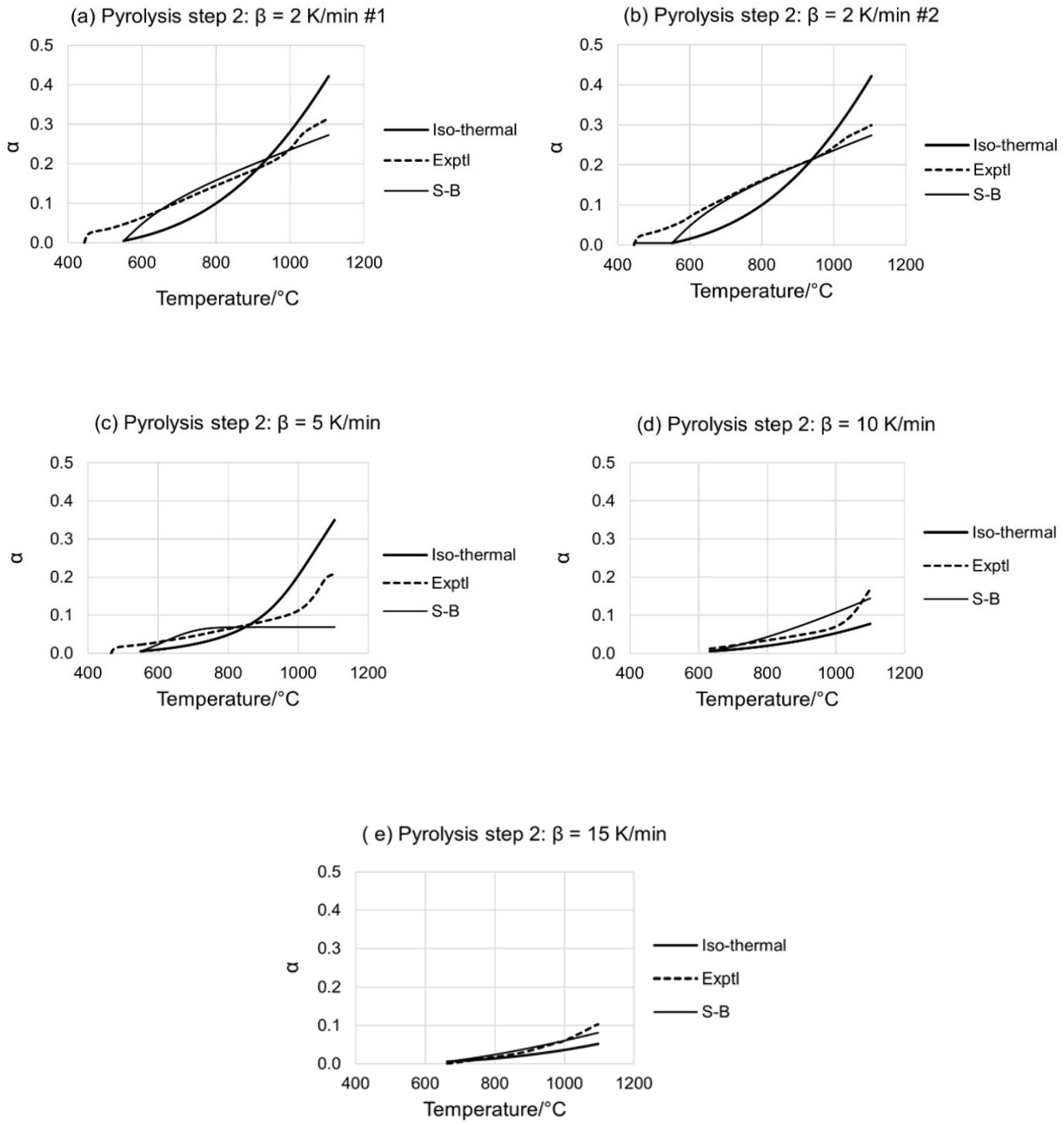

Figure 8: Second thermal event under pure N_2 Curves fitted individually for each heating rate.

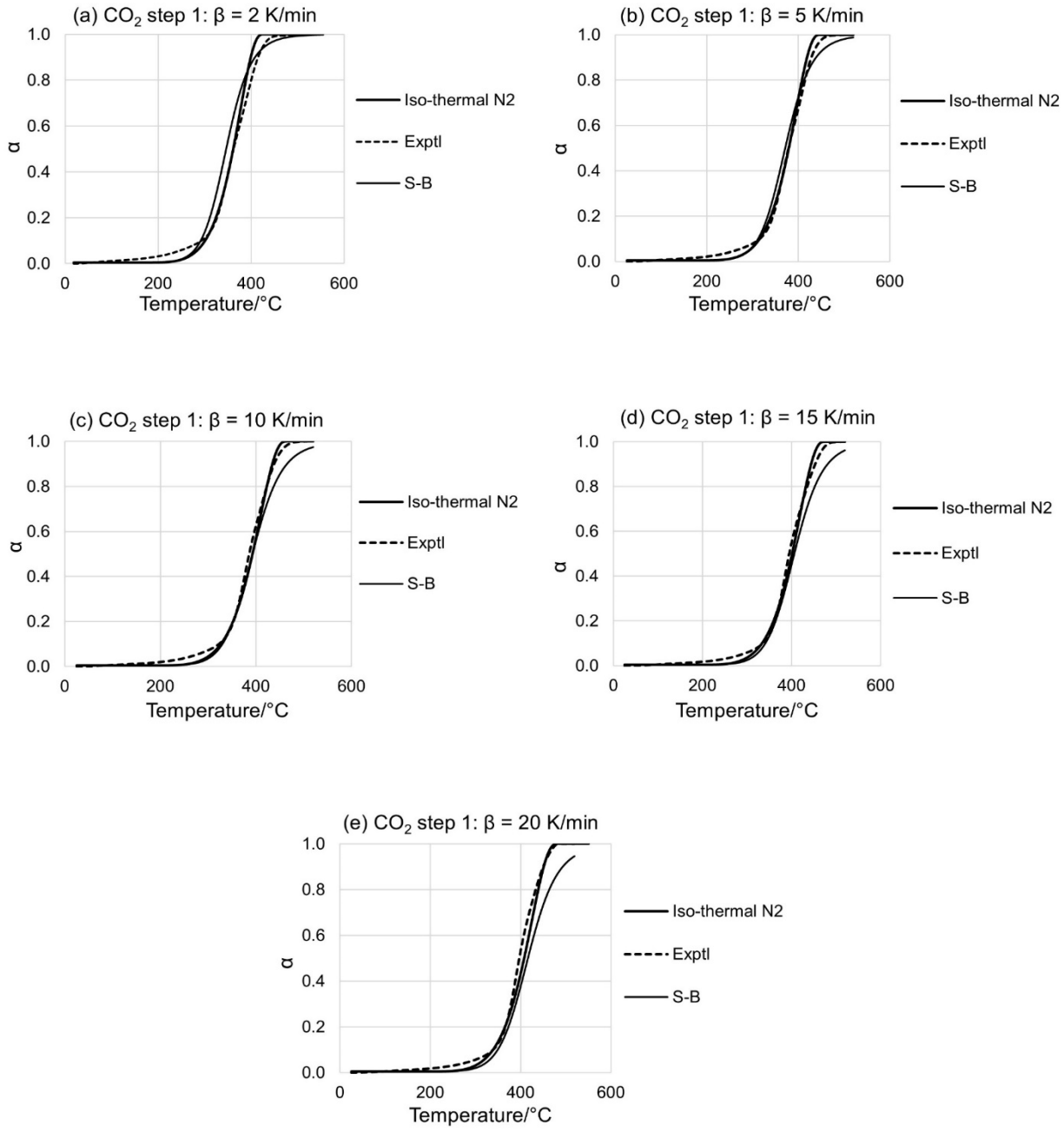

Figure 9: First thermal event, pyrolysis under CO_2. The lines marked 'Iso-thermal N_2' were obtained by direct non-linear model fitting of the corresponding nitrogen pyrolysis data. Curves fitted individually for each heating rate.

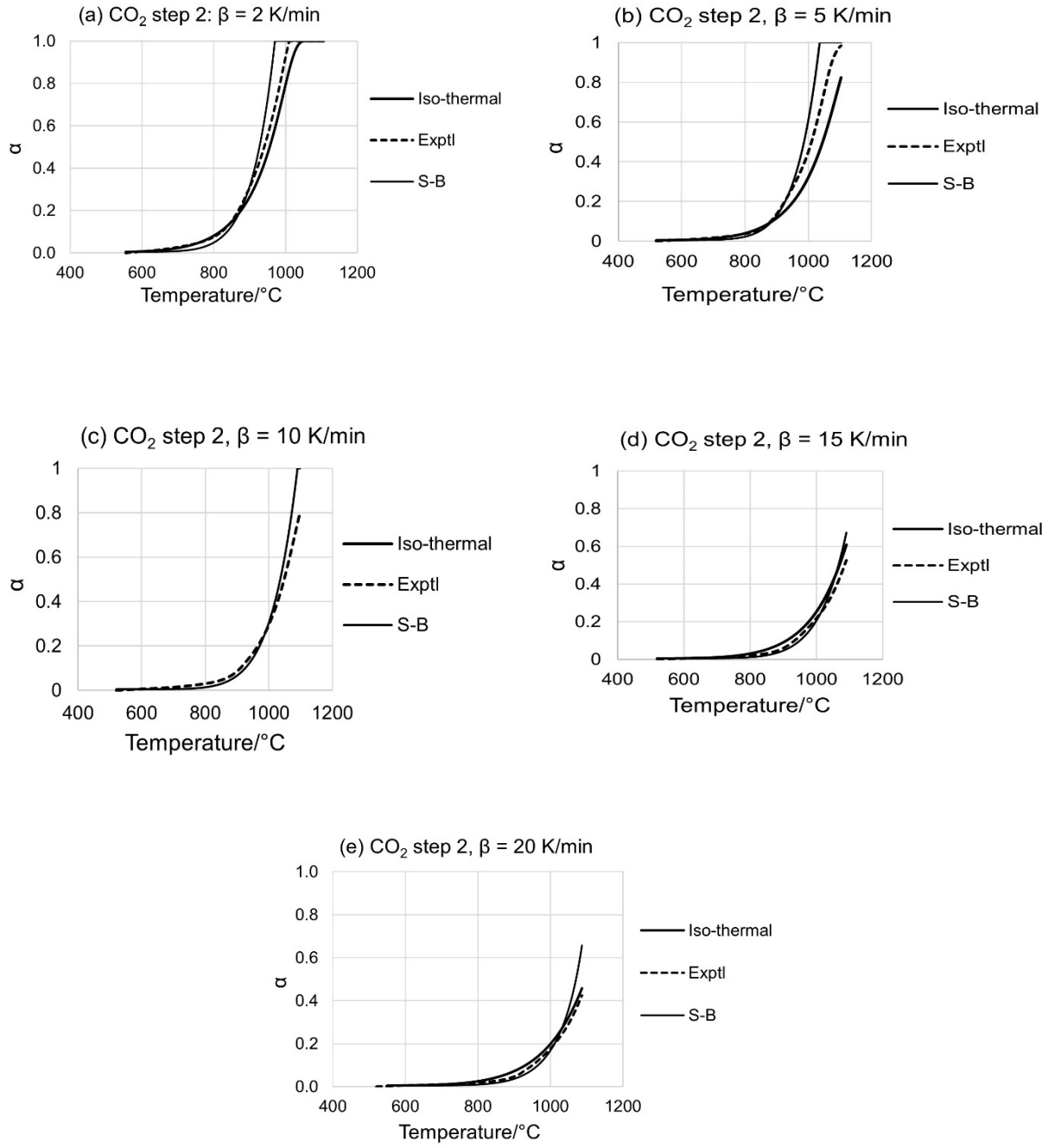

Figure 10: Second thermal event, gasification with CO_2 by the reverse Boudouard reaction at different heating rates. Curves fitted individually for each heating rate.

Table 5: Derived parameters for the Sestak-Berggren models.

S-B parameter	N_2 step 1	N_2 step 2	CO_2 step 1	CO_2 step 2
m	0	2.000×10^{-1}	3.335×10^{-2}	0
n	2.196	0	1.871	1.133×10^{-2}
p	7.410×10^{-5}	6.519×10^{-2}	2.146×10^{-5}	1.959×10^{-8}
q	0	0	0	5.930×10^{-2}
r	0	6.500×10^{-1}	7.952×10^{-4}	0
k_0 (min^{-1})	4.391×10^{8}	6.775×10^{-3}	3.882×10^{7}	1.751×10^{4}
E_A (kJ mol^{-1})	117.0	105.0	103.7	110.3

Table 6: Average absolute errors between experimental values and model simulations of dynamic thermograms.

Reaction	Iso-thermal	Sestak-Berggren
N_2 pyrolysis 200–550 °C	2.1 %	3.4 %
N_2 pyrolysis 550–1000 °C	1.6 %	2.5 %
CO_2 pyrolysis 200–550 °C	2.0 %	3.6 %
CO_2 reverse Boudouard 750–1100 °C	0.5 %	1.1 %

Although for engineering purposes the S-B models yielded acceptable errors, the isothermally derived models yielded clearly superior predictions in all cases.

There is always a possibility that limiting effects due to heat- or mass-transfer might influence predictions of chemical models. In order to assess this, approximations for the heating- and diffusion times derived from the analytical solutions, i.e., the error function, to Fourier and Fick's second law may be used [81]. To estimate the heating time the approximation is:

$$L = \sqrt{2\alpha_T \tau_H} \tag{9}$$

with L the characteristic length of the heat-flow path, τ_H the heating period, and α_T the thermal diffusivity expressed by:

$$\alpha_T = \frac{(1-\varepsilon)C_P\rho_B}{(1-\varepsilon)\kappa} = \frac{C_P\rho_B}{\kappa} \quad (10)$$

with C_P the heat capacity, ϱ_B the bulk density, κ the thermal conductivity, and the ε the voidage. The bulk density was determined to be 490 kg m^{-3}. Using the values 2010 J kg^{-1} K^{-1} and 0.09 W m^{-1} K^{-1} for the specific heat capacity and thermal conductivity respectively, and 2.5 mm, *i.e.* one half of the crucible diameter, the heating time is estimated to be of the order of 30–40 s. The diffusion time of the carbon dioxide from the top of the crucible to the sample bottom, may be estimated from:

$$L = \sqrt{2D\tau_D} \quad (11)$$

with D the self-diffusion constant. Using L = 5 mm as the height of the crucible and D as 2×10^{-5} m^2 s^{-1}, the diffusion time τ_D is estimated to be 0.1–1 s. A brief visual assessment of the thermograms, e.g. Figure 9 and Figure 10, indicates that the reaction times for the first pyrolysis step and the reverse Boudouard are roughly run between 150 min and 20 min for slow and high heating rates respectively. This is one to two orders of magnitude slower than the time required for the attainment of a homogeneous temperature distribution, and two to three orders of magnitude greater than the period required for the CO_2 to reach the reaction surface. It can thus be claimed with reasonable confidence that the deviation between simulation and experimental data is not attributable to heat- or mass-transfer effects. Cherbański et al. similarly conclude that heat conduction in samples < 100 mg has a negligible effect [80]. and Aylon et al. [82] conclude that for single particles smaller than 2 mm, the heat transfer rate has no discernible effect. This somewhat more pessimistic than the conclusion from this data analysis. A more reasonable suggestion for the poor prediction is that either the pre-exponential factor or the activation energy, or both, should be addressed as function of temperature or degree of conversion. Of course, the existence of more than one mechanism may also be a reason. In the case of the non-linear fit of the dynamic data, it was already done via the introduction of the α-dependence of the pre-exponential factor and the activation energy.

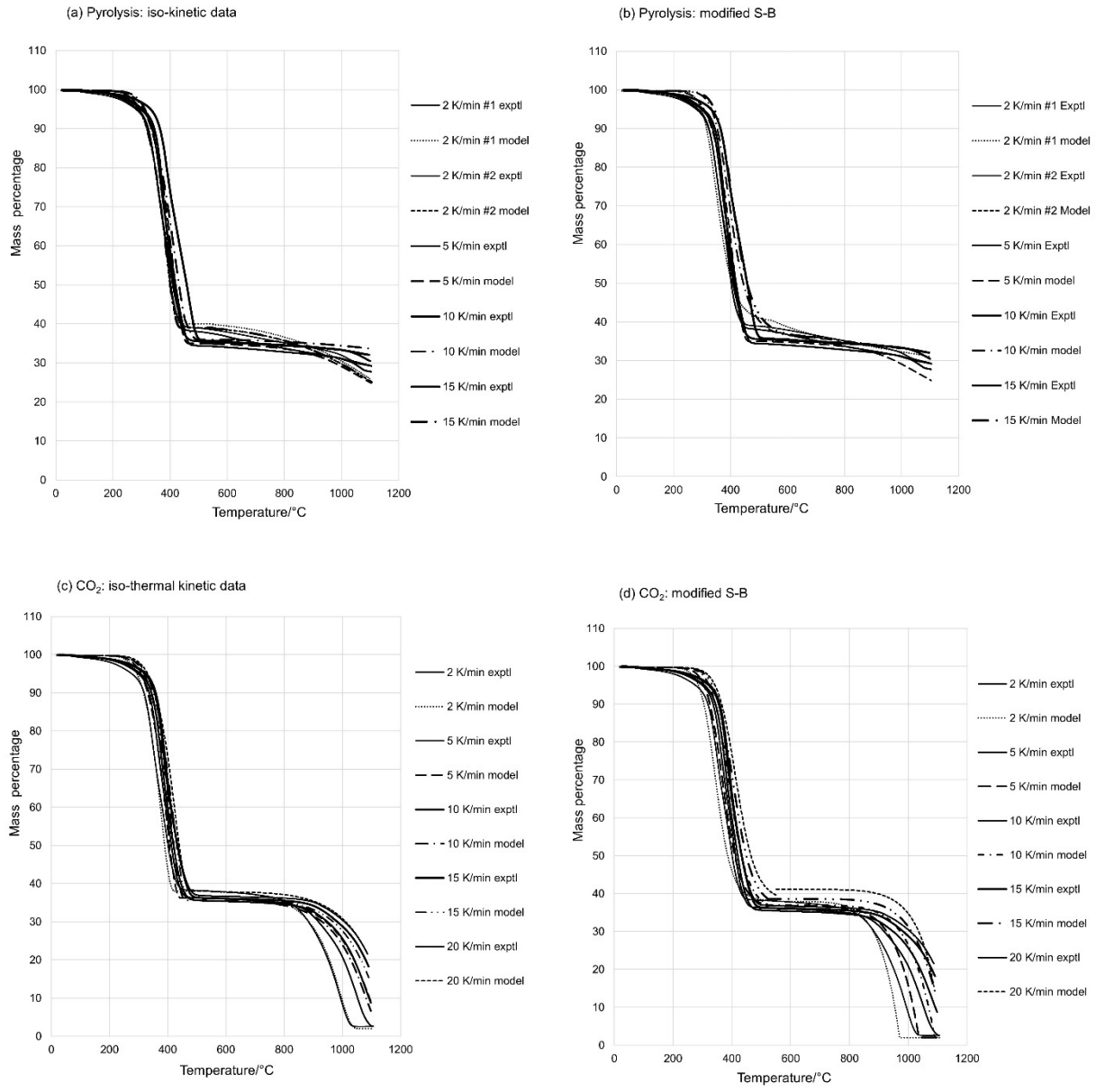

Figure 11: Simulation curves generated using the isokinetic parameters (a), (b) and the modified Sestak-Berggren from the dynamic analysis (c), (d) under pure N_2 and pure CO_2 respectively.

The general shape of the experimental TGA curves in Figure 3 and the shift to higher temperature with increasing heating rate are similar to those found in the literature, e.g., by Unapumnuk et al. [78], Seidelt et al. [79], and Cherbanski et al. [80]. The DTG curves applicable to the raw data are given in Figure 12 below

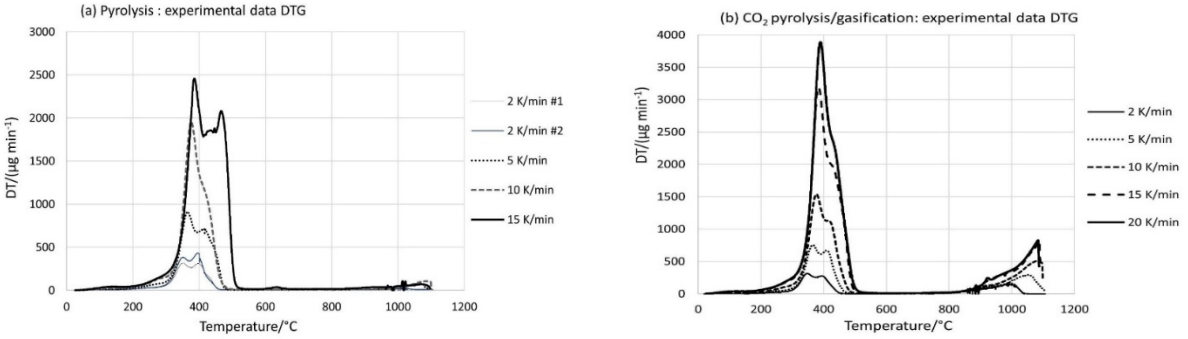

Figure 12: First derivatives of the pyrolysis (a) and reverse Boudouard (b) TG cuves.

As argued above, the shift to higher temperatures at higher heating rates is not attributable to heat transfer, but may rather be caused by a lag in the kinetics of the relevant reactions.

The DTG of tyre rubber shows distinct peaks which can be assigned to devolatilization, depolymerization and degradation of the additives. Figure 12(a) shows the typical pattern found for tyre rubber pyrolysis, with two major peaks attributable to the depolymerization of natural rubber (NR), butadiene rubber (BR) and styrene-butadiene rubber (SBR). The typical lateral shift in maxima associated with increasing heating rate was also observed here. Less reaction time at higher heating rates, causes the shift in both the rate of, and maximum mass loss [83]. The mass loss between 100 °C and 200 °C is attributable to the volatilization of plasticizers. [79,84]. The major peaks occurring at around 350–400 °C and 400–450 °C may be explained by reference to the work of Danon and co-workers [63] who showed by DTG and mass spectrometry of the pure compounds that NR, BR and SBR all exhibit consecutive primary and secondary devolatilization events. The DTG peaks could be correlated with the mass spectrometer MS ion current peaks of the main devolitalization products. During the primary event NR produced isoprene and dipentene, attributable to depolymerization, coinciding with the first DTG peak. The high-temperature shoulder was not assigned. In the case of BR and SBR two distinct ion current peaks were found – coinciding with the first and second DTG peaks – which could be correlated with the monomers butadiene and styrene. The thermolysis patterns for SBR and BR in tyre rubber are difficult to distinguish from each other due to the similarity in structure. However, the SBR content can be deduced from the styrene content in the off-gas [85]. Material from the same supplier, as used in this study, was employed in a TGA study by Cherop et al [86] for dynamic pyrolysis under N_2 at up to 600 °C. They observed no further mass loss above 500 °C. The DTG curves showed two maxima with the characteristic shift towards higher temperatures with increasing heating rate. In Figure 12(a) a further peak in the DTG curve is visible in the temperature region above 600 °C. This may be attributed to the devolatilization of sulphur-containing vulcanization residues remaining on the char [75]

Castaldi and Kwon [83] studied the thermal degradation of SBR at different heating rates under various atmospheres, including pure N_2. Degradation products identified by GC/MS consisted primarily of C_2–C_5 hydrocarbons and aromatic compounds. Pyrolysis in pure N_2 took place in the range of 230–430 °C and the off-gas contained relatively large amounts of C_4 hydrocarbons, mainly butane. Polyaromatic hydrocarbons (PAH) were observed at the high end of the temperature range, probably due to gas phase reactions involving the styrene component in SBR.

The thermolysis of tyre rubber under CO_2 atmosphere (Figure 12(b)) shows the same general trend as seen in Figure 12(a) with the exception that the DTG peaks are not well separated. Kwon and Castaldi [76] studied of the effect of CO_2 on the pyrolysis of SBR up to 700 °C. The concentrations of n-butane and styrene reached a maximum at 390 °C, which also corresponds to the maximum in the DTG curve. As the temperature rose, the initial C_4 hydrocabons in the off-gas began to give way to C_1–C_2 compounds, due to thermal cracking. This phenomenon was enhanced under CO_2 in comparison to N_2 atmosphere. The maximum concentration of styrene was also lower under CO_2 atmosphere. This may explain the presence of a shoulder, rather than a distinct second peak in the DTG curves shown above.

Cherop et al [86], using material from the same supplier as in this study, interpreted their experimental results by the Flynn-Wall-Osawa (FWO), Kissinger-Akahira-Sunrose (KAS) and Coats-Redfern methods. They found from the iso-conversional FWO and KAS treatment, an average E_A of 207 kJ mol^{-1}. In this study, E_a values of 117 kJ·mol^{-1} and 140 kJ·mol^{-1} were calculated by means of the Sestak-Berggren and Jander 3D diffusion models respectively for the same temperature range under N_2 flow, and E_A = 104 kJ mol^{-1} under CO_2 flow by the S-B model.

Danon et al. [87] applied a combination of model-based and model-free (Friedman, Kissinger type) devolatilization kinetics to a number of pure rubber components (NR, SBR, BR) as well as mixtures thereof and found E_A values of between 200 kJ mol^{-1} and 440 kJ mol^{-1}

Due to the variability of tyre rubber composition, experimental conditions, and the many modelling approaches, it is difficult to draw conclusions from comparisons of the kinetic parameters found in the literature, as summarized, e.g., by Quek and Balasubramanian [88], Menares et al. [84] and Lopez et al. [89]. Menares et al. [84] and Wang et al. [90] concluded that no single model can describe the entire thermolysis process. Determination of the pre-exponential factor in the Arrhenius equation by whichever model, is not feasible unless the model or mechanism has been determined beforehand [65].

A number of studies pertaining to the thermal analysis of the reverse Boudouard reaction has been published. The most pertinent publications are listed in Table 7.

Table 7: Comparison of kinetic data for the reverse Boudouard reaction.

Authors	Material	TGA regime	Model	E_A (kJ·mol^{-1})	P_{CO2} (atm)	Reference
Dutta et al.	Coal char	Isothermal	Reaction control, with intraparticle diffusion	248	1	[91]
Lee and Kim	Tyre char	Isothermal	*MVRM	238.9	0.3–1.0	[92]
Issac et al.	Tyre char	Isothermal	*RPM	174.9–177.0	1	[30]
Murillo et al.	Tyre char	Isothermal	*VM, MVM, CGSM, RPM	191.4–197.7	0.2–0.4	[93]
Betancur et al.	Tyre char	Isothermal	*CGSM, RPM, HMRPM	147.3–155.5	0.2–0.3	[94]
This work	Tyre char	Isothermal	*L3	201.7–223.1	1.0	

*MVRM - Modified Volume Reaction Model; RPM - Random Pore Model; VM - Volume reaction Model; MVM - Modified Volume reaction Model; CGSM - Changing Grain Size Model; HMRPM - Hybrid Modified Random Pore Model; L3 - Shrinking sphere, reaction control model.

Visual examination of the Arrhenius plot for the thermolysis under CO_2 atmosphere in **Error! Reference source not found.** shows a discontinuity in the data at roughly 840 °C; this may be interpreted as indicative of a change in the rate-determining step. This coincides with the rise in the high-temperature DTG curve (Figure 12(b)). This discontinuity is not seen in the Arrhenius plots reported by Issac et al. [30]. They started off with pre-charred tyre samples and argued that the relatively high E_A found is indicative of the slow reaction rate. Moreover, they found that the reactivity of an acid-washed char sample was higher than that of the untreated material, suggestive of a catalytic effect of the inorganic material in the latter. In the present study, however, the starting material was rubber and it can be expected that during the course of the observed reverse Boudouard reaction the solid char is still undergoing structural modification and degassing, i.e., that there is an effective continuous change in reaction conditions. In the present case, however, our aim is the extraction of a single, easily implementable model with reasonable predictive power, and thus a linear line fit for the full temperature range in the Arrhenius plot. Despite the data smoothing that this implies, the Levenspiel shrinking particle model with chemical reaction control (L3) for the reverse Boudouard in pure CO_2 atmosphere in the temperature range 750 °C to 1100 °C that gave the best fit, provides a physically meaningful description, with an activation energy of the same order of magnitude found by the researchers listed in Table 7.

The more complex models found in the literature, e.g., the Dutta model [91], modified volume reaction (MVRM) [92], changing grain size model (CGSM) and random pore model (RPM) [93] and hybrid modified random pore model (MHRPM) [94], require substantially more attention to the characterization of the solid.

Factors such as gas partial pressure, particle size, intraparticle diffusion, particle morphology, ash content and sample mass should be taken into account. The EA values found for the volume models were about 3 % lower than those for the grain size and random pore models, which in the context of this work, is acceptable for the simplification obtained for the modelling.

The kinetic parameters derived from the thermogravimetric data in this study, allow the rule-of-thumb prediction of the required reaction period as function of particle size and reactor temperature. This is important for our work, as an initial method to assess whether the kinetics data allow predictions of the correct order of magnitude. The assumptions made are: that the pyrolysis is diffusion controlled and its rate directly proportional to the surface area; that the reverse Boudouard reaction is controlled by the chemical reaction rate at the particle surface and the rate is directly proportional to the particle radius; that in both cases the inverse of the rate constant is the reaction time; and the full time required is the sum of the two reaction times. Results are displayed in Figure 13 below.

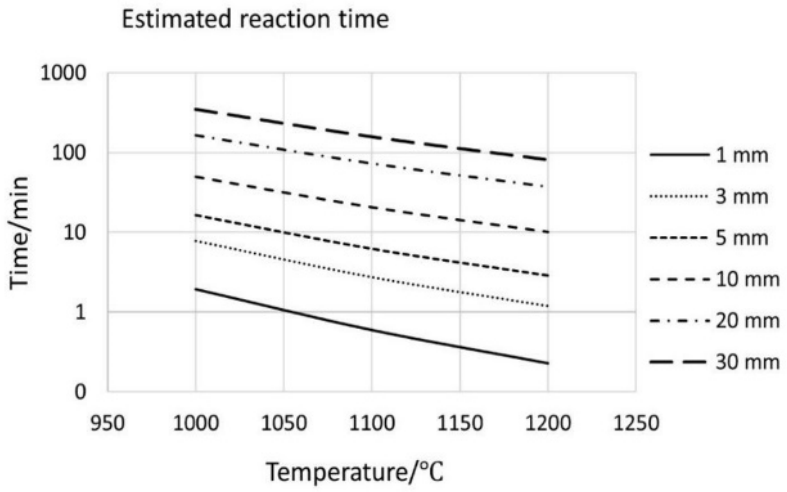

Figure 13: Time required for full reaction of rubber crumbs with pure CO_2, using iso-thermal parameters from this study.

In practice a plasma torch is used as heat source to control the reactor temperature at a constant temperature above 1000 °C. The results are in good agreement with our experience: at 1100–1200 °C pyrolysis and gasification of tyre crumbs are complete within a few minutes. Obviously, however, the estimated times to full gasification in the region of interest, i.e., for τ of the order of a few minutes, heat-transfer rates will be of the same order, and more detailed heat-transfer calculations will be required for higher accuracy.

4 Conclusions

It is possible to extract kinetic triplets from iso-thermal TGA data for the pyrolysis and CO_2-gasification of scrap-tyre rubber. The Arrhenius plots are not fully linear, suggesting several overlapping and complex individual reactions. In order to predict the thermal behaviour of the rubber under dynamic, i.e., non-iso-thermal, conditions using these data, refinement of the pre-exponential factors and activation energies is required. This was done by using the iso-thermal values as starting values for non-linear optimization, and assuming both to be functions of the degree of conversion. The average absolute error between experimental and model data, with the optimized parameters, is of the order of 2 %. An alternative approach yields a marginally worse accuracy; here the Sestak-Berggren equation was employed for direct non-linear model fitting to the full data set, i.e., for all heating rates, with random starting values, and again assuming a temperature dependence for the pre-exponential factor and activation energy. Despite its generality, the standard Sestak-Berggren model, with single values for the pre-exponential factor and the activation energy, was found to be inadequate to fit all heating rates simultaneously. All data processing and curve fitting was done using Excel's statistical and optimisation tools. The kinetic data will be used in future larger-scale research, focusing on the thermal histories of particles moving though a gasification reactor. The method is easily implementable and should provide useful pointers to researchers in rubber and scrap tyre recycling via gasification and/or pyrolysis.

Author statement

The roles of each author were as follows: AAJ - conceptualization, methodology, investigation, data curation, writing – original draft; IJvdW - methodology, supervision, project administration, funding acquisition, writing – review and editing; PLC – conceptualization, data curation, formal analysis, investigation, methodology, resources, software, visualization, writing – original draft.

Declaration of competing interests

We have no conflicts of interest to report.

Funding

AAJ thanks the University of Pretoria and the South African Academy for Science and Art for financial support.

5 References

[1] Goldstein Market Intelligence, in Goldstein Market Research Report, 2020. https://www.goldsteinresearch.com/report/global-tire-recycling-industry-market-tren ds-analysis. Accessed 2021/11/09.

[2] Basel Convention Technical Guidelines, in Technical Guidelines, UNEP Basel Convention, 2013. UNEP/SBC/2013/2. https://digitallibrary.un.org/record/750929?ln=en. Accessed 2021/12/06.

[3] Basel Convention Expert Working Group, Fact sheets on specific waste streams (UNEP/CHW/CLI_EWG.5/INF/5), at: Expert Working Group on Environmentally Sound Management, Fifth meeting, Bratislava, Slovakia, 13 – 15 July 2016, 38. http://www.basel.int/Implementation/CountryLedInitiative/Meetings/FifthmeetingoftheExpertWorkingGrouponESM/Overview/tabid/5189/Default.aspx. Accessed 2021/12/13

[4] A. Mohajerani, L. Burnett, J.V. Smith, S. Markovski, G. Rodwell, M.T. Rahman, H. Kurmus, M. M, A. Arulrajah, S. Horpibulsuk and F. Maghool, Recycling waste rubber tyres in construction materials and associated environmental considerations: A review, Resour. Conserv. Recycl., 155 (2020) 104679. https://doi.org/10.1016/j.resconrec.2020.104679.

[5] C. Pellegrino, F. Faleschini, C. Meyer, S. Mindess, Developments in the Formulation and Reinforcement of Concrete, Woodhead Publishing, 2019, p. 442, https://doi.org/10.1016/B978-0-08-102616-8.00002-2. Part I, Chapter 2.6 Accessed 2021/12/06.

[6] Rubber News Staff, in: Rubber News, May 4, 2018. https://www.rubbernews.com/article/20180504/NEWS/180509974/etrma-europe-recycling-94-of-its-used-tires. Accessed 2021/11/09.

[7] USEPA, in Facts and figures about materials, waste and recycling, United States Environmental Protection Agency, 2019. https://www.epa.gov/facts-and-figur es-about-materials-waste-and-recycling/durable-goods-product-specific-data#VehicleTires. Accessed 2021/12/06.

[8] A. Rowhani and T.J. Rainey, Scrap tyre management pathways and their use as a fuel – A review, Energies, 9, (2016) 888. https://doi.org/10.3390/en9110888.

[9] USEPA, in Tire-Derived Fuel, United States Environmental Protection Agency Archives, 2016. https://archive.epa.gov/epawaste/conserve/materials/tires/web/html/tdf.html. Accessed 2021/11/09.

[10] Portland Cement Association, in Tire-Derived Fuel, United States Environmental Protection Agency Archives, 2013. https://archive.epa.gov/epawaste/conserve/m aterials/tires/web/pdf/brochure5-08.pdf.

[11] S. Singh, W. Nimmo, B.M. Gibbs and P.T. Williams, Waste tyre rubber as a secondary fuel for power plants, Fuel, 88, (2009) 2473. https://doi.org/10.1016/j.fuel.2009.02.026.

[12] D. Czajczynska, R. Krzyzynska, H. Jouhara and N. Spencer, Use of pyrolytic gas from waste tire as a fuel: A review, Energy, 134, (2017) 1121. https://doi.org/10.1016/j.energy.2017.05.042.

[13] C. Hackett, T. Durbin, C. Bufalino, D. Gemmill and J. Pence, in Technology Evaluation and Economic Analysis of Waste Tire Pyrolysis, Gasification, and Liquefaction, California Environmental Protection Agency, (2006), 620-2006-0004. https://www.simekeninc.com/uploads/aK5HXQaL/CIWMB-Pyrolysis-Gasification-Report-6200 6004.pdf. Accessed 2021/12/03.

[14] M. Juma, Z. Koreňová, J. Markoš, J. Annus, L.L. Jelemenský, Pyrolysis and combustion of scrap tire, Petr. Coal 48 (2006) 15.

https://www.researchgate.net/profile/JumaHaydary/publication/26499998_Pyrolysis_and_combustion_of_Scrap_tyre/links/5585e11b08aeb0cdaddf6f91/Pyrolysis-and-combustion-o f-Scrap-tyre.pdf. Accessed 2021/12/13. ISSN 1337-7027.

[15] S.T. Kumaravel, A. Murugesan and A. Kumaravel, Tyre pyrolysis oil as an alternative fuel for diesel engines – A review, Renew. Sustain. Energy Rev., 60, (2016) 1678. https://doi.org/10.1016/j.rser.2016.03.035.

[16] M. Labaki and M. Jeguirim, Thermochemical conversion of waste tyres – a review, Environ. Sci. Pollut. Res., 24, (2017) 9962. https://doi.org/10.1007/s11356-016- 7780-0.

[17] W.M. Lewandowski, K. Januszewicz and W. Kosakowski, Efficiency and proportions of waste tyre pyrolysis products depending on the reactor type – A review, J. Anal. Appl. Pyrolys., 140 (2019) 25. https://doi.org/10.1016/j.jaap.2019.03.018.

[18] J.D. Martínez, R. Murillo and T. García, Production of carbon black from the waste tires pyrolysis in, Researchgate, 2013. https://www.researchgate.net/publication/283502434. Accessed 2021/12/06.

[19] E. Muzenda, in: Proceedings of the Int'l Confrence on Chemical Engineering & Advanced Computational Technologies (ICCEACT'2014), Pretoria (South Africa), 2014, in: http://iieng.org/images/proceedings_pdf/5240E1114021.pdf. Accessed 2021/12/06.

[20] B.O. Oboirien and B.C. North, A review of waste tyre gasification, J. Environ. Chem. Eng., 5, (2017) 5169. https://doi.org/10.1016/j.jece.2017.09.057.

[21] A. Quek and R. Balasubramanian, Liquefaction of waste tires by pyrolysis for oil and chemicals—A review, J. Anal. Appl. Pyrolys., 101, (2013) 1. https://doi.org/10.1016/j.jaap.2013.02.016.

[22] V. Torretta, E.C. Rada, M. Ragazzi, E. Trulli, I.A. Istrate and L.I. Cioca, Treatment and disposal of tyres: Two EU approaches. A review, Waste Manag. 45, (2015) 152. DOI, https://doi.org/10.1016/j.wasman.2015.04.018.

[23] P.T. Williams, Pyrolysis of waste tyres: A review, Waste Manag., 33, (2013) 1714. https://doi.org/10.1016/j.wasman.2013.05.003.

[24] N. Nkosi, E. Muzenda, T.A. Mamvura, M. Belaid and B. Patel, The development of a waste tyre pyrolysis production plant business model for the Gauteng Region, South Africa, Processes, 8, (2020). https://doi.org/10.3390/pr8070766.

[25] A. Mavukwana, C Sempuga, Recent developments in waste tyre pyrolysis and gasification processes, Chem. Eng. Commun., 2020. https://doi.org/10.1080/00986445.2020.1864624.

[26] M. Arabiourrutia, G. Lopez, M. Artetxe, J. Alvarez, J. Bilbao and M. Olazar, Waste tyre valorization by catalytic pyrolysis – A review, Renew. Sustain. Energy Rev., 129, (2020) 109932. https://doi.org/10.1016/j.rser.2020.109932.

[27] J.D. Martınez, N. Puy, R. Murillo, T. Garcı´a, M.V. Navarro and A.M. Mastral, Waste tyre pyrolysis– A review, Renew. Sustain. Energy Rev., 23, (2013) 179. https://doi.org/10.1016/j.rser.2013.02.038.

[28] J.M. Calo and M.T. Perkins, A heterogeneous surface model for the "steady-state" kinetics of the Boudouard reaction, Carbon, 25, (1987) 395. https://doi.org/10.1016/0008-6223(87)90011-X. Accessed 2021/12/06. .

[29] S. Ergun, Kinetics of the reaction of carbon dioxide with carbon, J. Phys. Chem., 60, (1956) 480. https://doi.org/10.1021/j150538a022.

[30] M. Issac, B. Dai and L. Zhang, Kinetics underpinning the C-CO_2 gasification of waste tyre char and its interaction with coal char upon co-gasification, Fuel, 256, (2019) 115991. https://doi.org/10.1016/j.fuel.2019.115991.

[31] P. Lahijani, Z.A. Zainal, M. Mohammadi and A.R. Mohamed, Conversion of the greenhouse gas CO_2 to the fuel gas CO via the Boudouard reaction: A review, Renew. Sustain. Energy Rev., 41, (2015) 615. https://doi.org/10.1016/j.rser.2014.08.034.

[32] N.R. Mitta, S. Ferrer-Nadal, A.M. Lazovic, J. Perales, E. Velo and L. Puigjaner, Modelling and simulation of a tyre gasification plant for synthesis gas production, Comput. Aided Chem. Eng., 21, (2006) 1771. https://doi.org/10.1016/S1570-7946(06)80304-4.

[33] P.A. Nikolaychuk and A.N. Kolesnikov, The study of compensation effect in reverse Boudouard reaction on graphite in presence of activating additives, ChemXpress, (5), (2014) 078. https://www.academia.edu/9296681/The_study_of_compensation_effect_in_reverse_Boudouard_reaction_on_graphite_in_presence_of_activating_additives. Accessed 2021/12/06.

[34] M. Policella, Z. Wang, K.G. Burra and A.K. Gupta, Characteristics of syngas from pyrolysis and CO_2-assisted gasification of waste tires, Appl. Energy , 254, (2019) 113678. https://doi.org/10.1016/j.apenergy.2019.113678.

[35] J. Preciado-Hernandez, J. Zhang, Z. M, Z. Zhang and D. Zhang, An experimental study of CO_2 gasification kinetics during activation of a spent tyre pyrolysis char, Chem. Eng. Res. Des., 149, (2019) 129. https://doi.org/10.1016/j.cherd.2019.07.007.

[36] S.A. Scott, J.F. Davidson, J.S. Dennis, P.S. Fennell and A.N. Hayhurst, The rate of gasification by CO_2 of chars from waste, Proceedings of the Combustion Institute, 30, (2005) 2151. https://doi.org/10.1016/j.proci.2004.08.061.

[37] R.P.W.J. Struis, C. von Scala, S. Stucki and R. Prins, Gasification reactivity of charcoal with CO_2. Part I: Conversion and structural phenomena, Chem. Eng. Sci., 57, (2002) 3581. https://doi.org/10.1016/S0009-2509(02)00254-3.

[38] R.P.W.J. Struis, C. von Scala, S. Stucki and R. Prins, Gasification reactivity of charcoal with CO_2. Part II: Metal catalysis as a function of conversion, Chem. Eng. Sci., 57, (2002) 3593. https://doi.org/10.1016/S0009-2509(02)00255-5.

[39] M. Hrabovsky, M. Konrad, V. Kopecky, M. Hlina, T. Kavka, O. Chumak, A. Maslani and G. Van Oost, Plasma aided gasification of biomass and plastics using CO_2 as oxidizer, in: International Symposium on Non-Thermal/Thermal Plasma Pollution Control Technology & Sustainable Energy, ISNTP 7*,* St. John´s, Newfoundland, Canada, 2010. https://www.researchgate.net/publication/266672217. Accessed 2021/11/10.

[40] I. Janajreh, S.S. Raza and A.S. Valmundsson, Plasma gasification process: Modeling, simulation and comparison with conventional air gasification, Energy Convers. Manag., 65, (2013) 801. https://www.researchgate.net/publication/266672217. Accessed 2021/12/06.

[41] P.G. Rutberg, V.A. Kuznetsov, A.N. Bratsev, V.E. Popov, S.V. Shtengel and A.A. Ufimtsev, Use of carbon dioxide in the chemical synthesis technologies, plasma gasification and carbon production, at: IOP Conference Series: Materials Science and Engineering, 2011. https://doi.org/10.1088/1757-899X/ 19/1/012003.

[42] R. Snoeckx and A. Bogaerts, Plasma technology – a novel solution for CO_2 conversion?, Chem. Soc. Rev., 46, (2017) 5805. https://doi.org/10.1039/c6cs00066e.

[43] L. Chen, L. Pershin and J. Mostaghimi, A new highly efficient high-power dc plasma torch, IEEE Trans. Plasma Sci. 36, (2008) 1068. https://doi.org/10.1109/TPS.2008.924405.

[44] J. Mostaghimi and M. Boulos, Thermal plasma sources: How well are they adopted to process needs?, Plasma Chem. Plasma Process., 35, (2015) 421. https://doi.org/10.1007/s11090-015-9616-y.

[45] M. Hrabovsky, Thermal plasma generators with water-stabilized arc, Open Plasma Phys. J., 2, (2009) 99. https://doi.org/10.2174/1876534300902010099.

[46] M. Hrabovsky, Steam plasma flows generated in Gerdien Arc: Environment for energy gas production from organics and for surface coatings, J. Fluid Sci. Technol., 6 (2011) 792. https://doi.org/10.1299/jfst.6.792.

[47] M. Hrabovsky, in; I. Matveev (Ed.), Plasma Assisted Combustion, Gasification, and Pollution Control, Vol 1- Methods of Plasma Generation for PAC, Outskirts Press Inc, Denver, CO, 2013, Chapter 2.3, p. 145. ISBN: 978-1-4327-8688-5.

[48] A.S. Lerner, Bratsev, A N, V.E. Popov, V.A. Kuznetsov, A.A. Ufimtsev, S.V. Shengel' and D.I. Subbotin, Production of hydrogen-containing gas using the process of steam plasma gasification of used tires, Glass Phys. Chem., 38, (2012) 511. https://doi.org/10.1134/S1087659612060041.

[49] H.S. Uhm, J.H. Kim and Y.C. Hong, Microwave steam torch, Appl. Phys. Lett. , 90, (2007) 211502. https://doi.org/10.1063/1.2742782.

[50] M. Hattingh, I.J. van der Walt and F.B. Waanders, Comparison of cyclone design methods for removal of fine particles from plasma generated syngas, Int. J. Mech. Aerosp. Ind. Mechatron. Manuf. Eng., 11, (2017) 19. https://publications.waset.org/10005989/comparison-of-cyclone-design-methods-for-removal-of-fine-particles-from-plasma-generated-syngas. Accessed 2021/11/10.

[51] N.P. Makaringe, I.J. van der Walt, G.L. Puts and P.L. Crouse, TGA-FTIR characterisation of bamboo wood, napier grass, pine wood and peach pips for gasification applications, Br. J. Therm. Anal., 6, (2017) 12. https://pdfs.semanticscholar.org/5902/ef5db3434251c6d925ed0d97562f1b9dff4a.pdf. Accessed 2021/12/06.

[52] R.F. Muvhiiwa, B. Sempuga, D. Hildebrandt and I. van der Walt, Study of the effects of temperature on syngas composition from pyrolysis of wood pellets using a nitrogen plasma torch reactor, J. Anal. Appl. Pyrolysis, 130, (2018) 159. https://doi.org/10.1016/j.jaap.2018.01.014.

[53] J.I. Osayi, S. Iyuke, M.O. Daramola, O. P, I.J. van Der Walt and S.E. Ogbeide, Chem. Eng. Commun., 205, (2018) 805. https://doi.org/10.1007/s11090-017-9786-x.

[54] I.J. van der Walt, A.A. Jansen and P.L. Crouse, Plasma-assisted treatment of municipal solid waste: A scenario analysis, Plasma Chem. Plasma Process., 37, (2017) 763. https://doi.org/10.1007/s11090-017-9786-x.

[55] A.W. Coats, J.P. Redfern, Thermogravimetric analysis - a review, Analyst, 88, (1963) 906 – 924. https://doi.org/10.1039/AN9638800906.

[56] S. Vyazovkin, A.K. Burnhamb, J.M. Criadoc, L.A. Pérez-Maqueda, C. Popescu and N. Sbirrazzuoli, ICTAC Kinetics Committee recommendations for performing kinetic computations on thermal analysis data, Thermochim. Acta 520 (2011) 1. https://doi.org/10.1016/j.tca.2011.03.034. Accessed 2021/12/06.

[57] S. Vyazovkin, K. Chrissafis, M.L. Di Lorenzo, N. Koga, M. Pijolat, B. Roduit, N. Sbirrazzuoli and J.J. Suñol, ICTAC Kinetics Committee recommendations for collecting experimental thermal analysis data for kinetic computations, Thermochim. Acta, 590 (2014) 1. https://doi.org/10.1016/j.tca.2014.05.036.

[58] O. Levenspiel, Chemical Reaction Engineering, 3rd Edition,1999, John Wiley and Sons, USA, p 566 – 582. ISBN 0-471-25424-X.

[59] D.C. Montgomery, Design and Analysis of Experiments, 9th Edition, 2017, John Wiley and Sons, Inc, Hoboken, NJ, ISBN: 9781119113478 (PBK) / ISBN: 9781119299455 (EVALC).

[60] Frontline Systems, http://solver.com. Accessed 2021/11/10.

[61] A. Alsaleh and M.L. Sattler, Waste tire pyrolysis: Influential parameters and product properties, Curr. Sustain. Renew. Energy Rep., 1, (2014) 129. https://doi.org/10.1007/s40518-014-0019-0.

[62] J. Alvarez, G. Lopez, M. Amutio, N.M. Mkhize, B. Danon, P. van der Gryp, J.F. Görgens, J. Bilbao and M. Olazar, Evaluation of the properties of tyre pyrolysis oils obtained in a conical spouted bed reactor, Energy, 128, (2017) 463. https://doi.org/10.1016/j.energy.2017.03.163.

[63] B. Danon, A. de Villiers and J.F. Görgens, Elucidation of the different devolatilisation zones of tyre rubber pyrolysis usingTGA-MS, Thermochim. Acta, 614, (2015) 59. https://doi.org/10.1016/j.tca.2015.05.012.

[64] M. Kyari, A. Cunliffe and P.T. Williams, Characterization of oils, gases, and char in relation to the pyrolysis of different brands of scrap automotive tires, Energy Fuels, 19, (2005) 1165. https://doi.org/10.1021/ef049686x.

[65] M. Wang, L. Zhang, A. Lei, M. Irfan, Y. Du and W. Di, Comparative pyrolysis behaviors of tire tread and side wall from waste tire and characterization of the resulting chars, J. Environ. Manag. , 232 (2019) 364. https://doi.org/10.1016/j.jenvman.2018.10.091.

[66] E.E. Kwon and M.J. Castaldi, Investigation of thermo-gravimetric analysis (TGA) on waste tires and chemical analysis including light hydrocarbons, substituted aromatics, and polycyclic aromatic hydrocarbon (PAH), in 15th North American Waste to Energy Conference, NAWTEC15-3218, ASME, Miami, Florida USA, 2007. https://doi.org/10.1115/NAWTEC15-3218.

[67] E.E. Kwon and M.J. Castaldi, Investigation of mechanisms of polycyclic aromatic hydrocarbons (PAH's) initiated from the thermal degradation of styrene butadiene rubber (SBR) in N_2 atmosphere, Environmetal Science and Technology, 42, (2008) 2175. https://doi.org/10.1021/es7026532.

[68] E.E. Kwon and M.J. Castaldi, Fundamental understanding of the thermal degradation mechanisms of waste tires and their air pollutant generation in a N_2 atmosphere Environ. Sci. Technol., 43, (2009) 5996. https://doi.org/10.1021/es900564b.

[69] F. Campuzano, A.G.A. Jameel, W. Zhang, A.-H. Emwas, A.F. Agudelo, J.D. Martínez and S.M. Sarathy, Fuel and chemical properties of waste tire pyrolysis oil derived from a continuous twin-auger reactor, Energy Fuels, 34 (2020) 12688−12702. https://doi.org/10.1021/acs.energyfuels.0c02271.

[70] G. Zhang, F. Chen, Y. Zhang, L. Zhao, J. Chen, L. Cao, J. Gao and C. Xu, Properties and utilization of waste tire pyrolysis oil: A mini review, Fuel Procss. Technol., 211, (2021) 106582. https://doi.org/10.1016/j.fuproc.2020.106582.

[71] J.A. Conesa, R. Font and A. Marcilla, Gas from the pyrolysis of scrap tires in a fluidized bed reactor, Energy Fuels, 10, (1996,) 134. https://doi.org/10.1021/ef950152t.

[72] M. Arabiourrutia, G. Lopez, G. Elordi, M. Olazar, R. Aguado and J. Bilbao, Product distribution obtained in the pyrolysis of tyres in a conical spouted bed reactor, Chem. Eng. Sci., 62 (2007) 5271. https://doi.org/10.1016/j.ces.2006.12.026.

[73] G. Lopez, J. Alvarez, M. Amutio, N.M. Mkhize, B. Danon, P. van der Gryp, J.F. Görgens, J. Bilbao and M. Olazar, Waste truck-tyre processing by flash pyrolysis in a conical spouted bed reactor, Energy Convers. Manag., 142, (2017) 523. https://doi.org/10.1016/j.enconman.2017.03.051.

[74] P.T. Williams and R.P. Bottrill, Pyrolysis-thermogravimetric analysis of tyres and tyre components, Fuel, 74, (1995) 736. https://doi.org/10.1016/0016-2361(94)00005-C .

[75] H. Hu, Y. Fang, H. Liu, R. Yu, G. Luo, W. Liu, A. Li and H. Yao, The fate of sulfur during rapid pyrolysis of scrap tires, Chemosphere, 97, (2014) 102. https://doi.org/10.1016/j.chemosphere.2013.10.037.

[76] E.E. Kwon, H. Yi and M.J. Castaldi, Mechanistic understanding of polycyclic aromatic hydrocarbons (PAHs) from the thermal degradation of tires under various oxygen concentration atmospheres, Environ. Sci. Technol., 46, (2012) 10752 − 10757. https://doi.org/10.1021/es301933p.

[77] D. Fauque, in Les professeurs du Conservatoire National des Arts et Métiers. Dictionnaire biographique 1794-1955, Institut national de recherche pédagogique, Paris 1994, p. 218. https://www.persee.fr/doc/inrp_0298-5632_1994_ant_19_1_8410. Accessed 2021/11/10.

[78] K. Unapumnuk, T.C. Keener and M. Lu, Pyrolysis behaviour of tire-derived fuels at different temperatures and heating rates, J. Air Waste Manag. Assoc., 56, (2006) 618. https://doi.org/10.1080/10473289.2006.10464481.

[79] S. Seidelt, M. Muller-Hagedorn and H. Bockhorn, Description of tire pyrolysis by thermal degradation: behaviour of main components, J. Anal. Appl. Pyrolysis, 75, (2006) 11. https://doi.org/10.1016/j.jaap.2005.03.002.

[80] R. Cherbański, K. Wróblewski and E. Molga, Chem. Proc. Eng., 38, (2017) 363. https://doi.org/10.1515/cpe2017-0028.

[81] J.R. Welty,. G.L. Rorrer, and D.G. Foster, Fundamentals of Momentum, Heat and Mass Transfer, 6th Edition, John Wiley & Sons, ISBN 1118808878.

[82] E. Aylon, M.S. Callen, J.M. Lopez, A.M. Mastral, R. Murillo, M.V. Navarro and S. Stelmach, Assessment of tire devolatilization kinetics, J. Anal. Appl. Pyrolysis 74, (2005) 259. doi:10.1016/j.jaap.2004.09.006.

[83] M.J. Castaldi and E. Kwon, An investigation into the mechanisms for styrene-butadiene copolymer (SBR) conversion in combustion and gasification environments, Int. J. Green Energy, 4, (2007) 45. https://doi.org/10.1080/15435070601015478.

[84] T. Menares, J. Herrera, R. Romero, P. Osorio and L.E. Arteaga-Pérez, Waste tires pyrolysis kinetics and reaction mechanisms explained by TGA and Py-GC/MS under kinetically-controlled regime, Waste Manag., 102, (2020) 21. https://doi.org/10.1016/j.wasman.2019.10.027.

[85] B. Danon and J. Görgens, Determining rubber composition of waste tyres using devolatilisation kinetics, Thermochimica Acta, 621, (2015) 56. https://doi.org/10.1016/j.tca.2015.10.008.

[86] P.T. Cherop, S.L. Kiambi and P. Musonge, Kinetics of granulated scrap tyre pyrolysis via thermogravimetry, in Proceedings of the Sustainable Research and Innovation Conference, 3 – 5 May JKUAT Main Campus, Kenya, 3 – 5 May 2017. https://www.researchgate.net/publication/328957267_Kinetics_of_granulated_scrap_tyre_pyrolysis_via_thermogravimetry. Accessed 2021/11/10.

[87] B. Danon, N.M. Mkhize, P. van der Gryp and J.F. Görgens, Combined model-free and model-based devolatilisation kinetics of tyre rubbers, Thermochim. Acta, 601, (2015) 45. https://doi.org/10.1016/j.tca.2014.12.003.

[88] A. Quek and R. Balasubramanian, Mathematical modeling of rubber tire pyrolysis, J. Anal. Appl. Pyrolysis, 95, (2012) 1. https://doi.org/10.1016/j.jaap.2012.01.012.

[89] F.A. López, A.A. El Hadad, F.J. Alguacil, T.A. Centeno and B. Lobato, Kinetics of the thermal degradation of granulated scrap tyres: A model-free analysis, Mater. Science (Medziagotyra), 19, (2013) 403. https://doi.org/10.5755/j01.ms.19.4.2947.

[90] C. Wang, B. Zhao, T. Tian, K. Wang, Z. Tian, W. Han and H. Bian, Study on the pyrolysis kinetics and mechanisms of the tread compounds of silica-filled discarded car tires, Polymers, 12, (2020) 810. https://doi.org/10.3390/polym12040810 .

[91] S. Dutta, C.Y. Wen and B.R. Johnson, Reactivity of coal and char. 1. In carbon dioxide atmosphere, Ind. Eng. Chem. Process Des. Dev., 16, (1977) 20. https://doi.org/10.1021/ie040026p.

[92] J.S. Lee and S.D. Kim, Gasification kinetics of waste tire-char with CO_2 in a thermobalance reactor, Energy 21, (1996) 343. https://doi.org/10.1016/0360-5442(95)00119-0.

[93] R. Murillo, M.V. Navarro, J.M. Lopez, E. Aylon, M.S. Callen, T. Garcıa and A.M. Mastral, Kinetic model comparison for waste tire char reaction with CO_2, Ind. Eng. Chem. Res., 43, (2004) 7768. https://doi.org/10.1021/ie040026p.

[94] M. Betancur, C.N. Arenas, J.D. Martínez, M.V. Navarro and R. Murillo, CO_2 gasification of char derived from waste tire pyrolysis: Kinetic models comparison, Fuel, 273, (2020). https://doi.org/10.1016/j.fuel.2020.117745.